MOX-Report No. 01/2020

Mathematical and numerical models of atherosclerotic plaque progression in carotid arteries

Pozzi, S.; Vergara, C.

MOX, Dipartimento di Matematica
Politecnico di Milano, Via Bonardi 9 - 20133 Milano (Italy)

mox-dmat@polimi.it http://mox.polimi.it

Mathematical and numerical models of atherosclerotic plaque progression in carotid arteries

Silvia Pozzi[1], Christian Vergara[2]

January 4, 2020

[1] MOX– Modellistica e Calcolo Scientifico
Dipartimento di Matematica, Politecnico di Milano silvia.pozzi@polimi.it

[4] LABS, Dipartimento di Chimica, Materiali e Ingegneria Chimica "Giulio Natta"
Politecnico di Milano christian.vergara@polimi.it

Keywords: Carotid arteries, atherosclerosis, plaque progression, low-density lipoprotein

Abstract

We propose a mathematical model for the description of plaque progression in carotid arteries. This is based on the coupling of a fluid-structure interaction problem, arising between blood and vessel wall, and differential problems for the cellular evolution. A numerical model is also proposed. This is based on the splitting of the coupled problem based on a suitable strategy to manage the multiscale-in-time nature of the problem. We present some preliminary numerical results both in ideal and real scenarios.

1 Introduction

Atherosclerosis consists in the formation of plaques at bifurcation sites. Carotid arteries are one of the preferential sites of atherosclerotic plaque formation. The main complications related to plaque formation are the partial or total occlusion of the internal carotids with consequent cerebral ischemia possibly leading to stroke, the rupture of the plaque with consequent embolization of fragments in the brain vessels, and the formation of a thrombus whose detachment leads to embolism.

The mechanism of plaque formation can be briefly summarized as follows. In regions where the viscous forces exerted by the fluid on the arterial wall (wall shear stresses, WSS) are low and oscillating, the permeability of the internal vessel layer (intima) to low-density lipoprotein (LDL) increases [10]. Once in the

intima, LDL can oxidize, leading to a pathological inflammation. To remove this, macrophages are recruited. Due to the ingestion of large amounts of oxidized LDL, macrophages differentiate into foam cells, which are responsible for the growth of a sub-endothelial plaque. If this inflammatory process persists for a sufficient time, the plaque can emerge in the lumen. In Figure 1, left, these steps are schematically reported.

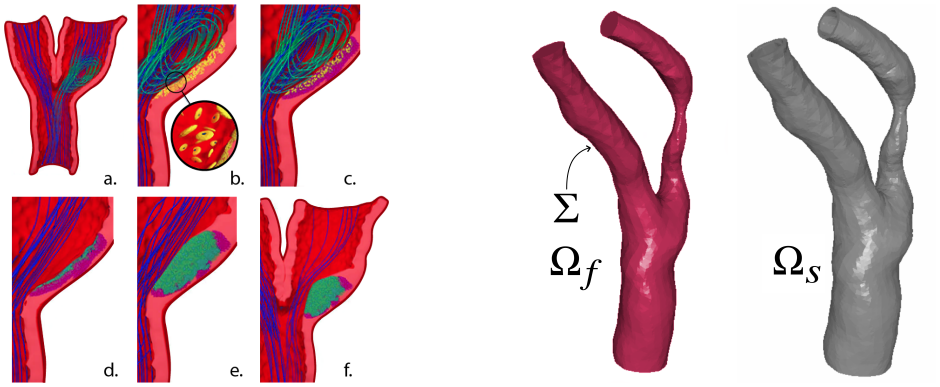

Figure 1: Left: Schematic view of plaque formation and progression. a) Carotid with blood ricirculation; b) LDL (in yellow) penetrates in the vessel wall; c) oxidized LDL (in purple); d-e-f) macrophages (in green) accumulate. Right: fluid and structure computational domains.

The prediction of the formation and evolution of the plaque in carotids is of utmost importance. For this reason, in recent years some studies have focused on the mathematical description of plaque progression [1,5,17]. The main characteristics that a mathematical model should account for are:

i. A detailed description of blood dynamics, which plays a crucial role in plaque progression;

ii. A description of the mutual dependence between macro and micro spatial scales;

iii. The coupling between models describing events that occur with different characteristic times, that is seconds (blood dynamics) and years (plaque progression).

Regarding point i, some works consider blood dynamics in rigid walls [1, 2, 5], whereas more recent studies include fluid-structure interaction (FSI) to better describe blood dynamics and include a growth tensor in the vessel wall dynamics to account for the plaque development [15, 16] (point ii, *micro-to-macro* scales feedback). Another choice consists in using a plaque growth law [1,2,5,17]. Regarding the *macro-to-micro* scales feedback in point ii, most of the studies derive a relation between WSS and variation of permeability of cellular

quantities [1, 5, 15]. A wide class of works considers a macroscopic description of cellular events by means of suitable partial differential equations (PDEs) for LDL, macrophages and foam cells evolution [1, 2, 5, 15, 16], whereas other works consider for them a cellular description [17]. Regarding point iii, we point out that no specific techniques have been considered so far to manage the different temporal scales. We also notice that most of the works consider ideal geometries for the numerical experiments [1, 2, 5, 16], whereas in [15] an application to real geometries of mice is considered.

Starting from the studies cited above, in this work we propose a mathematical model for plaque progression in carotids, based on an FSI model, PDEs for LDL, macrophages and foam cells evolution, spatial feedbacks between macro and micro scales based on WSS and a growth law. At the numerical level, we propose a new strategy to deal with the multiscale-in-time nature of the problem. The model is applied to 3D cases, both in ideal and real geometries.

2 Mathematical models

The mathematical model for plaque progression is based on two groups of differential problems and on their coupling. In the first group, we consider the "short time scale" model, that is the FSI problem, in the unknowns fluid velocity and pressure ($\boldsymbol{u}$, p) and structure displacement $\boldsymbol{d}$, which occurs with a characteristic time of 1 second (the heartbeat). In the second group, we have the "long time scales" models, interacting with one another, that is two time dependent diffusion-reaction (DR) problems for LDL and macrophages concentrations (c_{LDL} and c_{macr}) [1, 15] and one ordinary differential equation (ODE) for the foam cells concentration c_{FC} [5].

The coupling between these two groups of models is provided by the time-averaged WSS (TAWSS), which influences the LDL and macrophages permeabilities [1] (*macro-to-micro* feedback) and by c_{FC}, which determines the plaque growth $\boldsymbol{d}_G$ [17] (*micro-to-macro* feedback). In Figure 2 we report a diagram of the mathematical model. Notice that the fluid and structure domains Ω_f and Ω_s depend on the plaque growth $\boldsymbol{d}_G$.

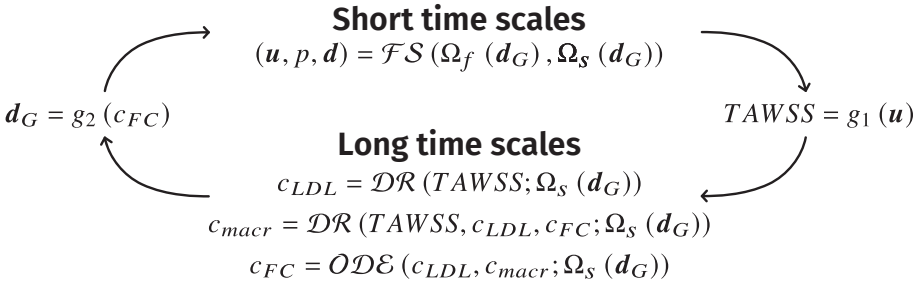

Figure 2: Diagram of the mathematical model of plaque progression.

Referring to Figure 1, right, we detail in what follows the equations of the submodels.

- **FSI problem**:

$$\begin{cases} \rho_f \left(\partial_t \boldsymbol{u} + \boldsymbol{u} \cdot \nabla \boldsymbol{u}\right) - \nabla \cdot \boldsymbol{T}_f(\boldsymbol{u}, p) = \boldsymbol{0} & \text{in } \Omega_f(\boldsymbol{d}, \boldsymbol{d}_G), \\ \nabla \cdot \boldsymbol{u} = 0 & \text{in } \Omega_f(\boldsymbol{d}, \boldsymbol{d}_G), \\ \boldsymbol{u} = \partial_t \boldsymbol{d} & \text{on } \Sigma(\boldsymbol{d}, \boldsymbol{d}_G), \\ \boldsymbol{T}_f(\boldsymbol{u}, p)\boldsymbol{n} = \boldsymbol{T}_s(\boldsymbol{d})\boldsymbol{n} & \text{on } \Sigma(\boldsymbol{d}, \boldsymbol{d}_G), \\ \rho_s \partial_{tt} \widehat{\boldsymbol{d}} - \nabla \cdot \widehat{\boldsymbol{T}}_s = \boldsymbol{0} & \text{in } \widehat{\Omega}_s(\boldsymbol{d}_G), \end{cases} \tag{1}$$

together with initial and boundary conditions and where ρ_f and ρ_s are the fluid and structure densities, $\boldsymbol{T}_f = \mu(\nabla \boldsymbol{u} + (\nabla \boldsymbol{u})^T)\boldsymbol{n} - p\boldsymbol{I}$ is the fluid Cauchy stress tensor, μ the fluid viscosity, $\widehat{\boldsymbol{T}}_s$ is the wall first Piola-Kirkhhoff tensor representing an hyperelastic material, $\boldsymbol{n}$ is the unit normal vector, and $\widehat{\ }$ denotes quantities in the Lagrangian framework;

- **Time-averaged wall shear stress**:

$$TAWSS = \frac{1}{T} \int_0^T \mu \sum_{j=1}^{2} \sqrt{\left(\left(\nabla \boldsymbol{u} + (\nabla \boldsymbol{u})^T \right) \boldsymbol{n} \cdot \boldsymbol{\tau}_j \right)^2 dt} = g_1(\boldsymbol{u}), \tag{2}$$

with $\boldsymbol{\tau}_j$ the tangential unit vectors;

- **Cellular differential problems**:

$$\begin{cases} \partial_t c_{LDL} - \nabla \cdot (D_{LDL} \nabla c_{LDL}) + r_{ox} c_{LDL} = 0 & \text{in } \Omega_s(\boldsymbol{d}_G), \\ \zeta_{LDL} c_{LDL} - D_{LDL} \nabla c_{LDL} \cdot \boldsymbol{n} = -\zeta_{LDL} c_{LDL,f} & \text{on } \Sigma(\boldsymbol{d}, \boldsymbol{d}_G), \\ \zeta_{LDL} = \dfrac{\zeta_{LDL}^{ref}}{ln(2)} ln\left(1 + \dfrac{2TAWSS^{ref}}{TAWSS + TAWSS^{ref}}\right); \end{cases} \tag{3}$$

$$\begin{cases} \partial_t c_{macr} - \nabla \cdot (D_{macr} \nabla c_{macr}) + (r_{ox} c_{LDL})\, c_{macr} = 0 & \text{in } \Omega_s(\boldsymbol{d}_G), \\ \zeta_{macr} c_{macr} - D_{macr} \nabla c_{macr} \cdot \boldsymbol{n} = -\zeta_{macr} c_{macr,f} & \text{on } \Sigma(\boldsymbol{d}, \boldsymbol{d}_G), \\ \zeta_{macr} = \dfrac{\zeta_{macr}^{ref}}{ln(2)} ln\left(1 + \dfrac{31/30 TAWSS^{ref}}{TAWSS + 1/30 TAWSS^{ref}}\right), \\ D_{macr} = D_{macr}^{dis} + \left(D_{macr}^{healthy} - D_{macr}^{dis}\right) e^{-c_{FC}}; \end{cases} \tag{4}$$

$$\partial_t c_{FC} = r_{ox} c_{LDL} c_{macr} \qquad \text{in } \Omega_s(\boldsymbol{d}_G), \tag{5}$$

where D are the diffusion tensors, r_{ox} the oxidation rate, ζ the permeabilities, index ^{ref} means reference, index ^{dis} means diseased. Notice that both diffusion-reaction problems are equipped by a Robin condition at the interface Σ to account for the equilibrium with the fluid concentrations, which are here supposed to be known constants ($c_{LDL,f}$, $c_{macr,f}$) ;

- Growth function

$$\boldsymbol{d}_G = \kappa c_{FC} \boldsymbol{n} = g_2(c_{FC}) \qquad \text{on } \Sigma(\boldsymbol{d}_G), \tag{6}$$

that is a growth of the interface that occurs in the normal direction and where κ is a parameter regulating the growth rate [17]. The growth $\boldsymbol{d}_g$ is then extended in the whole $\Omega_s(\boldsymbol{d}_g)$ by means of an harmonic extension.

3 Numerical methods

For the numerical solution of the coupled problem (1)-(2)-(3)-(4)-(5)-(6), we propose a way to treat its multiscale-in-time nature, that in fact decouples the subproblems (FSI, LDL, macrophages, foam cells) which could be solved by means of separate/pre-existing codes. This strategy is summarized in Figure 3.

The blue region, characterized by a time discretization parameter Δt, is devoted to the discretized-in-time long time scale problems (3)-(4)-(5), which are solved for K time instants at the current block m in the domain $\Omega_{s,m-1}$ obtained at the previous block.

After K time steps we update the structure domain by means of (6), obtaining $\Omega_{s,m}$ and then we solve for J heartbeats the discretized-in-time FSI problem (1) in this domain and in the corresponding fluid domain, with a discretization parameter $\Delta\tau << \Delta t$ (yellow region). After J heartbeats, we compute TAWSS by means of (2) and we update accordingly the permeabilities ζ_{LDL} and ζ_{macr}. Then the new block $m+1$ starts. These steps are detailed in Algorithm 1.

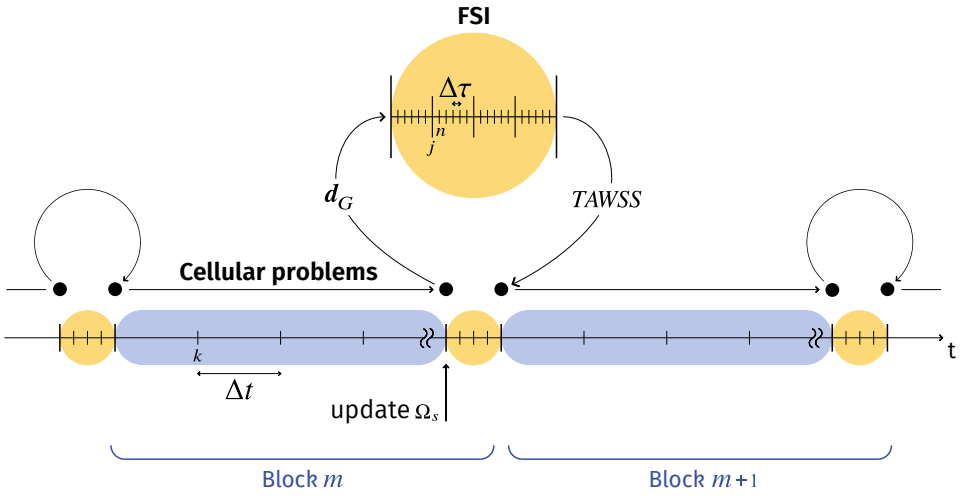

Figure 3: Schematic representation of the numerical treatment of the multiscale-in-time coupled problem.

Algorithm 1 *Numerical solution of the plaque progression coupled problem*

Let m be the block index, j the heartbeat index, n the short scales time step index, k the long scale time step index.

for $m = 1 : M$ **do**

for $k = 1 : K$ **do**

Solve the discretized-in-time cellular problems at block m, time instant k:

$$\begin{aligned} c^k_{LDL,m} &= \mathcal{DR}^k(TAWSS_{m-1}; \Omega_{s,m-1}), \\ c^k_{macr,m} &= \mathcal{DR}^k(TAWSS_{m-1}, c^k_{LDL,m}, c^{k-1}_{FC,m}; \Omega_{s,m-1}), \\ c^k_{FC,m} &= \mathcal{ODE}^k(c^k_{LDL,m}, c^k_{macr,m}, \Omega_{s,m-1}); \end{aligned}$$

end for

Update the structure domain:

$$\boldsymbol{d}_{G,m} = g_2(c_{FC,m}), \qquad \Omega_{s,m} = \Omega_{s,m-1} + \boldsymbol{d}_{G,m};$$

for $j = 1 : J$ **do**

for $n = 1 : N$ **do**

Solve the discretized-in-time FSI problem at heartbeat j, time instant n:

$$\left(\boldsymbol{u}^{j,n}_m, p^{j,n}_m, \boldsymbol{d}^{j,n}_m\right) = \mathcal{FS}\left(\Omega^{j,n-1}_{f,m-1}, \widehat{\Omega}_{s,m-1}\right);$$

end for

end for

Compute the TAWSS:

$$TAWSS_m = g_1\left(\boldsymbol{u}_m\right).$$

end for

We discuss in what follows the numerical strategies used for the solution of both the cellular and FSI subproblems.

Regarding cellular problems, we consider BDF1 for time discretization and P1 Finite Elements for space discretization; linearization of the subproblems is performed by an explicit treatment of c_{FC} in the evolution of macrophages, whereas the other non-linearities are solved by the sequential solution of the 3 subproblems, see Algorithm 1.

For the numerical solution of the FSI problem we consider a first order time discretization for fluid, structure and kinematic conditions, with a semi-implicit treatment of the fluid convective term. The fluid geometry problem is determined by means of an harmonic extension of the interface displacement in an *Arbitrary Lagrangian-Eulerian* formulation [6, 9], whereas the geometric coupling is treated explicitly, a strategy which is known to be stable and accurate in hemodynamics, see e.g. [7, 11, 12, 14]. The resulting FSI problem is solved monolithically by means of P2-P1 Finite Elements, with an inexact Newton method given by a block approximation of the Jacobian, leading to the split solution of fluid velocity, pressure and vessel wall unknowns, see [3, 4]. This method has been shown to be highly scalable in the hemodynamic regime.

All the strategies have been implemented in the Finite Elements library *LifeV* (www.lifev.org).

4 Numerical results

We present in what follow some 3D preliminary numerical results. In all the experiments we considered the linear Hooke law for the structure constitutive relation with Young modulus $E = 3 \cdot 10^5\, Pa$ and Poisson ratio $\nu = 0.49$. We used the following values for the other physical parameters: $\rho_f = 1.0\, g/cm^3$, $\rho_s = 1.1\, g/cm^3$, $\mu = 0.035\, P$, $D_{LDL} = 1.2 \cdot 10^{-7}\, cm^2/s$, $r_{ox} = 0.5 \cdot 10^{-2}\, s^{-1}$, $c_{LDL,f} = 1.9 \cdot 10^{-3}\, g/cm^3$, $\zeta_{LDL}^{ref} = 1.7 \cdot 10^{-11}\, cm/s$, $c_{macr,f} = 5 \cdot 10^{-5}\, g/cm^3$, $\zeta_{macr}^{ref} = 1.1 \cdot 10^{-12}\, cm/s$ [1], $D_{macr}^{dis} = 5.0 \cdot 10^{-9}\, cm^2/s$, $D_{macr}^{healthy} = 1.0 \cdot 10^{-9}\, cm^2/s$ [16]. Moreover, we set $\Delta t = 3\, h$, $\Delta\tau = 10^{-3}\, s$, $J = 3$, $N = 800$, $K = 750$ (corresponding to about 3 months). The value of $TAWSS^{ref} = 2.1\, Pa$ has been estimated by the Poiseuille solution.

At the inlet, we prescribed a physiological representative flow rate taken from [8], whereas at the outlet sections we considered absorbing boundary conditions [13].

In the first experiment, we consider as initial configuration an ideal vessel given by a cylinder of radius $0.5\, cm$ and length $6.5\, cm$, where a 60% eccentric stenosis of length $1.8\, cm$ has been included $2.5\, cm$ far from the inlet. This leads to recirculation regions downstream the stenosis, leading to low values of TAWSS that should induce the mechanism of LDL, macrophages and foam cells accumulation.

From the results reported in Figure 4, we observe in fact that, in correspondence of regions of low TAWSS given by the stagnation of blood flow, a growth of about $0.2\, mm$ occurs after block 2, that is after 6 months. These results, although qualitative, show that our methodology is stable from the numerical point of view and that it is able to produce significant plaque growth values which are in the expected ranges.

In the second experiment, we apply the proposed method to a real carotid reconstructed from MRI data. In this case, we start from a healthy geometric condition and we expect that possibly stagnation regions at the bifurcation may lead to plaque growth. This is confirmed by the results reported in Figure 5, where TAWSS is very low in correspondence of recirculation regions and, accordingly, plaque growth occurs. These results highlight the ability of our method to be applied to real scenarios, allowing to obtain significant results from the quantitative point of view ($0.1\, mm$ in 6 months).

These results are preliminary and are the first step towards a concrete application of our method. Of course validation of the method is mandatory. To this aim, comparisons of the results with clinical analysis of patients before and after the plaque progression shall be considered.

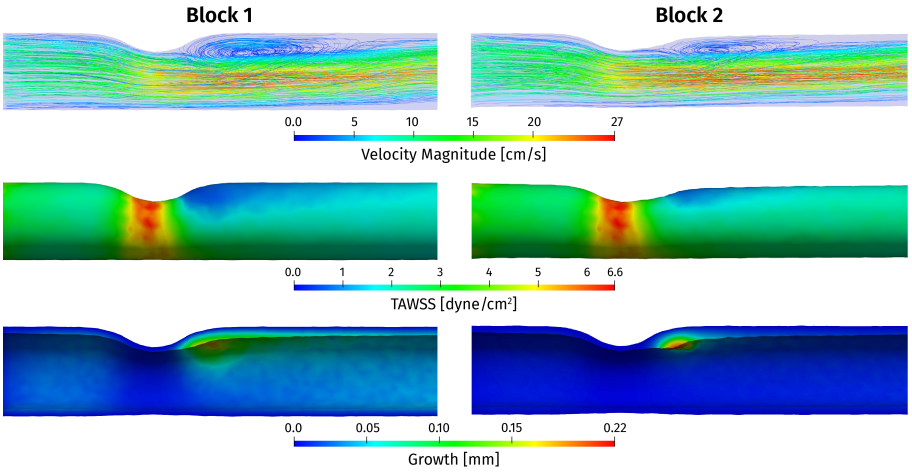

Figure 4: Top: Streamlines of blood velocity field. Middle: TAWSS. Bottom: Plaque growth. Left: Block 1. Right: Block 2.

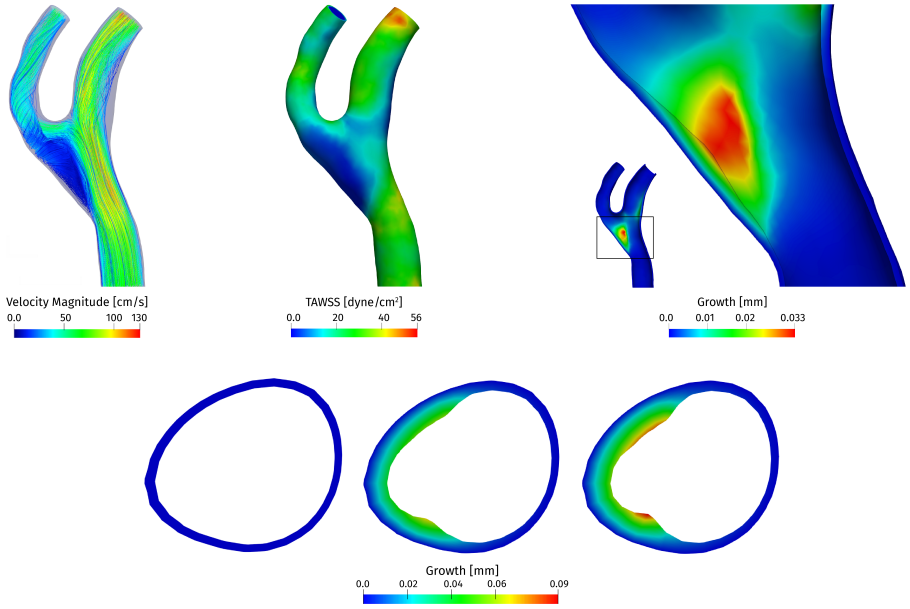

Figure 5: Top: Streamlines of blood velocity (left), TAWSS (middle), plaque growth (right), block 1. Bottom: Plaque growth on a section at the bifurcation at the starting time instant (left), after block 1 (middle) and after block 2 (right).

References

[1] V. Calvez, J.G. Houot, N. Meunier, A. Raoult, and G. Rusnakova. Mathematical and numerical modeling of early atherosclerotic lesions. *ESAIM: Proceedings*, 30, 2010.

[2] M. Cilla, E. Peña, and M. Martínez. Mathematical modelling of atheroma plaque formation and development in coronary arteries. *Journal of the Royal Society, Interface / the Royal Society*, 11:20130866, 2014.

[3] P. Crosetto, S. Deparis, G. Fourestey, and A. Quarteroni. Parallel algorithms for fluid-structure interaction problems in haemodynamics. *SIAM J. Sci. Comput.*, 33:1598–1622, 2011.

[4] S. Deparis, D. Forti, G. Grandperrin, and A. Quarteroni. Facsi: A block parallel preconditioner for fluid-structure interaction in hemodynamics. *J. Comput. Physics*, (327):700–718, 2016.

[5] G. Di Tomaso, V. Diaz-Zuccarini, and C. Pichardo-Almarza. A multiscale model of atherosclerotic plaque formation at its early stage. *IEEE transactions on bio-medical engineering*, 58:3460–3, 2011.

[6] J. Donea, S. Giuliani, and J.P. Halleux. An arbitrary lagrangian-eulerian finite element method for transient dynamic fluid-structure interactions. *Computer Methods in Applied Mechanics and Engineering*, 33:689–723, 09 1982.

[7] M.A. Fernández, J.F. Gerbeau, and C. Grandmont. A projection semi-implicit scheme for the coupling of an elastic structure with an incompressible fluid. *Int. J. Num. Methods Engrg.*, 69(4):794–821, 2007.

[8] B. Guerciotti, C. Vergara, L. Azzimonti, L. Forzenigo, A. Buora, P. Biondetti, and M. Domanin. Computational study of the fluid-dynamics in carotids before and after endarterectomy. *Journal of Biomechanics*, 49, 11 2015.

[9] C.W Hirt, A.A Amsden, and J.L Cook. An arbitrary lagrangian-eulerian computing method for all flow speeds. *Journal of Computational Physics*, 14:227–253, 03 1974.

[10] D. Ku, D. Giddens, C. Zarins, and S. Glagov. Pulsatile flow and atherosclerosis in the human carotid bifurcation - positive correlation between plaque location and low and oscillating shear-stress. *Arteriosclerosis (Dallas, Tex.)*, 5:293–302, 05 1985.

[11] F. Nobile, M. Pozzoli, and C. Vergara. Time accurate partitioned algorithms for the solution of fluid-structure interaction problems in haemodynamics. *Computers and Fluids*, 86, 11 2013.

[12] F. Nobile, M. Pozzoli, and C. Vergara. Inexact accurate partitioned algorithms for fluid-structure interaction problems with finite elasticity in haemodynamics. *Journal of Computational Physics*, 273:598–617, 2014.

[13] F. Nobile and C. Vergara. An effective fluid-structure interaction formulation for vascular dynamics by generalized robin conditions. *SIAM J. Scientific Computing*, 30:731–763, 01 2008.

[14] E.W. Swim and P. Seshaiyer. A nonconforming finite element method for fluid-structure interaction problems. *Comput. Methods Appl. Mech. Engrg.*, 195(17–18):2088–2099, 2006.

[15] M. Thon, A. Hemmler, A. Glinzer, M. Mayr, M. Wildgruber, A. Zernecke-Madsen, and M. Gee. A multiphysics approach for modeling early atherosclerosis. *Biomechanics and Modeling in Mechanobiology*, 17, 2017.

[16] Y. Yang, M. Jager, W.and Neuss-Radu, and T. Richter. Mathematical modeling and simulation of the evolution of plaques in blood vessels. *Journal of mathematical biology*, 72, 2015.

[17] T. Zohdi, G. Holzapfel, and S.A. Berger. A phenomenological model for atherosclerotic plaque growth and rupture. *Journal of theoretical biology*, 227:437–43, 2004.

MOX Technical Reports, last issues

Dipartimento di Matematica
Politecnico di Milano, Via Bonardi 9 - 20133 Milano (Italy)

57/2019 Antonietti, P.F.; Bertoluzza, S.; Prada, D.; Verani M.
The Virtual Element Method for a Minimal Surface Problem

58/2019 Antonietti, P.F; Manzini, G.; Mourad, H.M.; Verani, M.
The virtual element method for linear elastodynamics models. Design, analysis, and implementation

59/2019 Antonietti, P.F; Manzini, G.; Mourad, H.M.; Verani, M.
The virtual element method for linear elastodynamics models. Design, analysis, and implementation

60/2019 Ieva, F; Paganoni, A.M.; Romo, J.; Tarabelloni, N.
roahd Package: Robust Analysis of High Dimensional Data

56/2019 Antonietti, P.F.; Berrone, S.; Borio A.; D'Auria A.; Verani, M.; Weisser, S.
Anisotropic a posteriori error estimate for the Virtual Element Method

55/2019 Agosti, A.; Ciarletta, P.; Garcke, H.; Hinze, M.
Learning patient-specific parameters for a diffuse interface glioblastoma model from neuroimaging data

54/2019 Simona, A.; Bonaventura, L; de Falco, C.; Schoeps, S.
IsoGeometric Approximations for Electromagnetic Problems in Axisymmetric Domains

53/2019 Cerroni, D., Penati, M.; Porta, G.; Miglio, E.; Zunino, P.; Ruffo, P.
Multiscale modeling of glacial loading by a 3D Thermo-Hydro-Mechanical approach including erosion and isostasy

52/2019 Cerroni, D.; Radu, A. R. ; Zunino, P.
Numerical solvers for a poromechanic problem with a moving boundary

51/2019 Parolini, N.; Riccobene, C.; Schenone, E.
Reduced models for liquid food packaging systems